Physica **121A** (1983) 457–478 *North-Holland Publishing Co.*

EXPERIMENTS ON THE VISCOSITY OF SOME SYMMETRIC TOP MOLECULES IN THE PRESENCE OF MAGNETIC AND ELECTRIC FIELDS

E. MAZUR*, E. VISWAT, L.J.F. HERMANS and J.J.M. BEENAKKER

Huygens Laboratorium der Rijksuniversiteit, Leiden, The Netherlands

Received 27 April 1983

In order to obtain information on the scalar structure of non-equilibrium polarizations a comparison between the magnetic and the electric field effect on the viscosity of some symmetric top molecules has been carried out. It is shown that the polarization produced in viscous flow is more complicated than assumed so far.

1. Introduction

Experimental studies on the influence of external magnetic fields on transport properties of dilute polyatomic gases have been carried out extensively during the last decade (see, e.g., refs. 1–3). The occurrence of these so-called Senftleben–Beenakker effects is explained in the following way. A macroscopic gradient in a polyatomic gas not only produces an anisotropy in the velocity distribution but via collisions also anisotropies (or polarizations) in the angular momentum distribution. Such angular momentum dependent polarizations, which are produced in collisions because of the non-spherical intermolecular potential, can be partially destroyed by applying an external field which will cause the molecules to precess around the field direction. This in turn will alter the transport properties.

Polarizations constitute deviations of the molecular distribution f from the local Maxwellian f^0. Their general form[4]) is given by $\boldsymbol{\Phi}^{pq} = (2^p/p!)^{1/2}[\boldsymbol{W}]^p \mathscr{Y}^{(q)}(\boldsymbol{J})$, a tensor consisting of an irreducible[5–7]) tensor of rank p in the reduced molecular velocity $\boldsymbol{W}$ and a normalized irreducible tensor of rank q in the angular momentum $\boldsymbol{J}$, multiplied by a scalar factor P depending on W^2, J^2 and $J_\parallel$,

$$\mathscr{Y}^{(q)}(\boldsymbol{J}) = (2q+1)^{1/2} \frac{[\boldsymbol{J}]^q}{\{[\boldsymbol{J}]^q \odot [\boldsymbol{J}]^q\}^{1/2}}.$$

The tensorial factors of the various polarizations observed in field effects are by now well known. For linear diamagnetic $^1\Sigma$ molecules the tensorial factor is

* Present address: Gordon McKay Laboratory, Harvard University, Cambridge, MA 02138, USA.

0378-4371/83/0000–0000/$03.00

directly related to the field dependence of the effect. The scalar factor however, on which we will concentrate in this paper and which is less accessible experimentally, remains undetermined. This factor is usually expanded into orthogonal polynomials and generally only the first polynomial is taken into account. The study of symmetric top molecules might give some information since for these molecules, in contrast to linear $^1\Sigma$ molecules, the precession frequencies depend on the rotational state. Hence the way in which an external field influences the transport properties depends on P. For such a study experiments on the viscosity are preferable to other transport properties for the following reasons. Earlier experiments showed that in viscous flow only one type of angular momentum dependent polarization plays a role for most gases. A disentanglement of contributions from various polarizations is therefore not needed and a straightforward analysis of the scalar factor is possible. An additional advantage is gained by the fact that the polarization observed in viscosity experiments is a polarization with irreducible tensorial part $\mathscr{Y}^{(2)}(\boldsymbol{J})$. Polarizations observed in other transport phenomena[8]) have more than one irreducible part and therefore a more complicated decay mechanism.

So far, for the scalar factor P of the $\mathscr{Y}^{(2)}$ type of polarization, two possible choices have been considered[9]):

1) $P = 1$: since the tensor $\mathscr{Y}^{(2)}$ is normalized only the orientation of the angular momentum plays a role ("normalized").

2) $P = \dfrac{\sqrt{\boldsymbol{J}^2(\boldsymbol{J}^2 - \frac{3}{4})}}{\langle \boldsymbol{J}^2(\boldsymbol{J}^2 - \frac{3}{4})\rangle_0^{1/2}}$: $\boldsymbol{J}$ is treated in analogy to $\boldsymbol{W}$, i.e., magnitude as well as orientation are considered and the tensor polarization essentially has the form $[\boldsymbol{J}]^2$. Henceforth this choice will shortly be denoted by $P \sim \boldsymbol{J}^2$ ("unnormalized"). For $J > 2$ this reduces to $P = \boldsymbol{J}^2/\langle \boldsymbol{J}^4\rangle_0^{1/2}$, where $\langle\ \rangle_0$ denotes the equilibrium average of a quantity.

Experiments on the influence of a magnetic field on the viscosity of some symmetric top molecules have already been carried out by Van Ditzhuyzen[9]). Similar experiments were carried out in an electric field[10-12]). Unfortunately, it was not possible from these measurements to determine the exact form of the polarization. The results seemed to favour slightly the so-called unnormalized form, but an unambiguous choice could not be made. In this respect a comparison between magnetic and electric field effects looks more promising. The underlying reason is that the spread in precession frequencies that occurs for symmetric top molecules in an electric field is different from that in a magnetic field (see section 2). The differences in the shapes of the resulting field effect curves are rather subtle however, which makes it desirable to perform the experiments in one apparatus in order to eliminate systematic errors.

The following section gives the theoretical expressions, then follows a description of the experimental set-up in sections 3 and 4, and, finally, the results are presented and discussed in sections 5 and 6.

2. Theory

Theoretical expressions for the influence of external fields on viscosity have been derived by McCourt and Snider[13]) and Kagan[14]). In this section we will only deal with the relevant expressions, for a detailed outline of the theory one is referred to refs. 13, 14 and 4.

The polarization observed in viscosity experiments[15 17,9]) is a tensor polarization with tensorial factor $\mathscr{Y}^{(2)}$. The only exception known so far is formed by NH_3 and ND_3 where a $[\boldsymbol{W}]^2\,\mathscr{Y}^{(1)}$-polarization plays a dominant role. If we restrict ourselves to the cases where only the $\mathscr{Y}^{(2)}$ is present, the spherical components of the viscosity tensor change in the presence of a magnetic field according to

$$\frac{\Delta\eta_\mu}{\eta} = -\frac{\mathfrak{S}^2\binom{20}{02\pi}}{\mathfrak{S}(20)\mathfrak{S}(02\pi)}\left\langle P^2[f(\mu\xi_{02\pi}) + \mathrm{i}g(\mu\xi_{02\pi})]\right\rangle_0, \tag{1}$$

where the field-dependent functions are

$$f(x) = \frac{x^2}{1+x^2}, \qquad g(x) = \frac{x}{1+x^2}, \tag{2}$$

and the field parameter

$$\xi_{02\pi} = \frac{\omega}{n\langle v\rangle_0 \mathfrak{S}(02\pi)} \equiv \omega\tau_{02\pi}. \tag{3}$$

For even-in-field coefficients this reduces to

$$\frac{\eta_\mu^+ - \eta(0)}{\eta(0)} = \mathrm{Re}\,\frac{\Delta\eta_\mu}{\eta} = -\frac{\mathfrak{S}^2\binom{20}{02\pi}}{\mathfrak{S}(20)\mathfrak{S}(02\pi)}\left\langle P^2 f(\mu\xi_{02\pi})\right\rangle_0. \tag{4}$$

Here, $\mathfrak{S}\binom{20}{02\pi}$ and $\mathfrak{S}(02\pi)$ are effective cross sections for the production and decay of the 02π-polarization as defined in ref. 4, $\mathfrak{S}(20)$ a cross section related to the field free viscosity $\eta(0)$, $\langle v\rangle_0$ the average thermal speed and ω the Larmor frequency.

For isotropic systems in an electric field, coefficients which are odd in the field vanish due to the fact that the electric field is a polar vector. The change in the even-in-field coefficients is given by eq. (4). Thus, both magnetic and electric field effects are described by eq. (4), yet with different precession frequencies. For symmetric top molecules in magnetic and electric fields those frequencies are given

by

$$\omega_B = \frac{g_\perp \mu_N}{\hbar}\left[1 + \frac{g_\parallel - g_\perp}{g_\perp}\frac{K^2}{J(J+1)}\right]B \tag{5}$$

and

$$\omega_E = \frac{\mu_e}{\hbar}\frac{K}{J(J+1)}E, \tag{6}$$

respectively; $g_\perp$ and $g_\parallel$ are the rotational g-factors perpendicular and parallel to the figure axis, μ_N the nuclear magneton, μ_e the electric dipole moment of the molecule, and J and K the rotational quantum numbers corresponding to the angular momentum J and its projection upon the figure axis $J_\parallel$, respectively. The equilibrium average of any angular momentum dependent quantity A is defined by the expression

$$\langle A(J,K)\rangle = \sum_{J=0}^{\infty}\sum_{K=-J}^{K=+J} A(J,K)(2J+1)\exp\left\{-\frac{\hbar^2}{2I_\perp kT}\left[J(J+1)+\left(\frac{I_\perp}{I_\parallel}-1\right)K^2\right]\right\} \Bigg/ \sum_{J=0}^{\infty}\sum_{K=-J}^{K=+J}(2J+1)\exp\left\{-\frac{\hbar^2}{2I_\perp kT}\left[J(J+1)+\left(\frac{I_\perp}{I_\parallel}-1\right)K^2\right]\right\}, \tag{7}$$

which is to be applied in eqs. (1) and (4), and where the I are the moments of inertia of the molecule.

From eqs. (5) and (6) it follows that for symmetric top molecules the precession frequency around the field direction depends on the rotational (J, K)-state of the molecule. For the magnetic field case the spread in precession frequencies depends on the difference between $g_\perp$ and $g_\parallel$ and is usually small[9]). For the electric field case, the spread is necessarily large, since the precession frequency is proportional to $K/J(J+1)$ and vanishes for $K = 0$, irrespective of the value of the electric dipole moment of the molecule. The field dependence of the viscosity coefficients for symmetric top molecules will be given by a weighted sum of contributions from molecules with different precession frequencies. The weight factor is a product of the Maxwellian weight of the rotational state and the scalar factor P of the tensor polarization, as can be seen from eqs. (1) and (4). The difference in behaviour between magnetic and electric field effects, due to the difference in the spread of precession frequencies, makes a comparison of the two types of measurements a powerful tool in the discrimination between different forms of P. This is illustrated in fig. 1 where the calculated ratio of E/p to B/p for the η_1^+ coefficient of CH_3F is plotted as a function of the degree of saturation (i.e., the ratio of the change

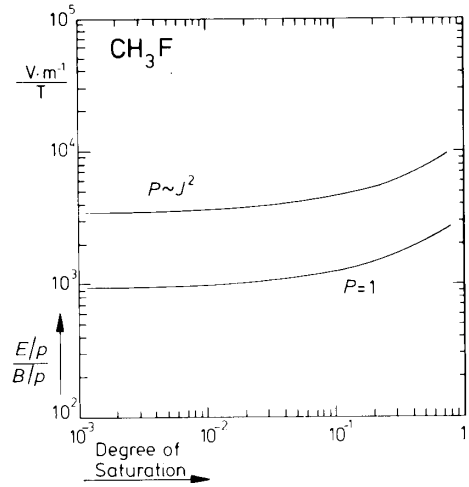

Fig. 1. The calculated ratio of E/p to B/p for the η_1^+ viscosity coefficient of CH_3F plotted as a function of the degree of saturation of the effect (see text). Two possible choices of the scalar factor P of the $\mathscr{Y}^{(2)}$-polarization are shown.

in the coefficient at the current field to the saturation value). There is a large difference between the curves calculated for the two different choices of P in use so far.

It should be stressed that two assumptions have been made in the derivation of eq. (1). First, the relaxation time $\tau_{02\pi}$ is described by a state-averaged cross section. Secondly, contributions from other polarizations are assumed to be absent. This last assumption can readily be checked experimentally if two different coefficients η_1^+ and η_2^+ are measured. When only a polarization of tensorial structure $\mathscr{Y}^{(2)}$ is present, the ratio of the "positions" B/p of the two coefficients should result in a horizontal line $(B/p)_1/(B/p)_2 = 2$, see eq. (4) and, e.g., fig. 4.

3. Description of the experimental set-up

For accurate measurements of small changes in the viscosity an apparatus consisting of four identical capillaries of rectangular cross section arranged in a Wheatstone bridge is appropriate. Fig. 2a shows a schematic view of the apparatus, which is very similar to the one used by Van Ditzhuyzen[9]). The capillaries (length $l = 60$ mm, width $w = 10$ mm, thickness $t = 0.5$ mm), consist of two gold coated brass plates held apart by pyrex spacers, see fig. 2b. The gold coating minimizes adsorption effects and protects the optically polished surfaces of the plates against corrosive gases.

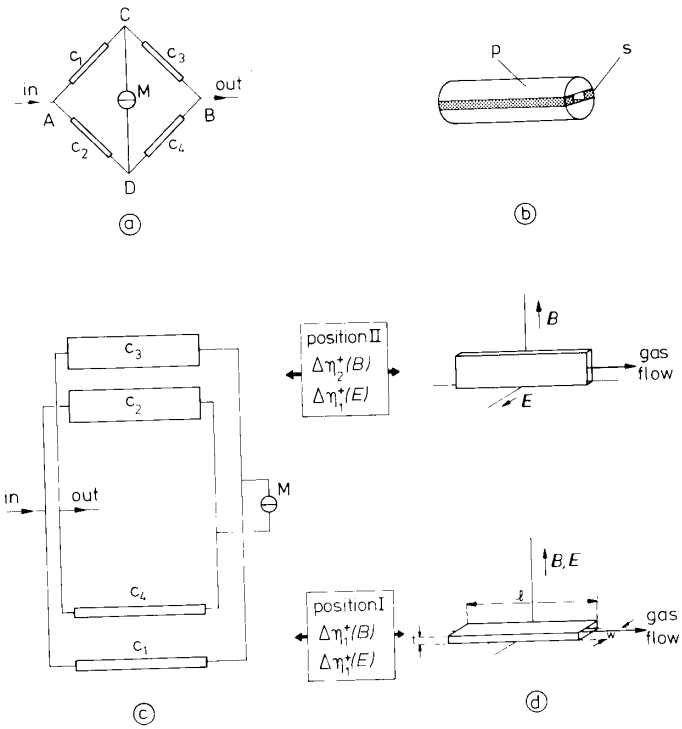

Fig. 2. The apparatus for the measurement of $\Delta\eta_1^+$ and $\Delta\eta_2^+$ in magnetic and $\Delta\eta_1^+$ in electric fields. a) Schematic diagram of the Wheatstone bridge consisting of four identical capillaries. M = differential manometer, c_1, c_2, etc. = capillaries. b) View of one of the capillaries. s = pyrex spacer, p = gold coated plate. c) The arrangement of the capillaries in the apparatus. Either the pair c_1 and c_4 (position I) or the pair c_2 and c_3 (position II) is positioned in the centre of the vertical magnetic field. Distance between upper and lower pair of capillaries: 0.62 m. d) The orientation of the capillaries with respect to the fields. Dimensions of the capillaries: $l = 60$ mm, $w = 10$ mm, $t = 0.5$ mm.

For measurements in electric fields a voltage difference (up to 1 kV) is applied to the plates of the pair of capillaries c_1 and c_4 (or the pair c_2 and c_3). The change in viscosity is then given by a ratio of pressure differences,

$$2\frac{p_C(E) - p_D(E)}{p_A - p_B} = -\frac{\Delta\eta_1^+(E)}{\eta}. \tag{8}$$

The subscripts A, B, C and D denote the corresponding points of the bridge as shown in fig. 2a.

For measurements in magnetic fields the apparatus is placed in the 0.1 m room temperature bore of a 7.6 T superconducting magnet (homogeneity 99%). In order to determine more than one component of the viscosity tensor a design as shown

in fig. 2c was chosen. By positioning either the pair c_1 and c_4 (position I) or the differently orientated (see fig. 2d) pair c_2 and c_3 (position II) in the field centre, two different components of the viscosity tensor can be measured. According to Hulsman et al.[18]) the field induced imbalance of the bridge is now related to changes in the viscosity by

$$2\frac{p_C(B)-p_D(B)}{p_A-p_B} = -\frac{\Delta\eta_1^+(B)}{\eta} \quad \text{(position I)}, \tag{9}$$

$$2\frac{p_D(B)-p_C(B)}{p_A-p_B} = -\frac{\Delta\eta_2^+(B)}{\eta} \quad \text{(position II)}. \tag{10}$$

Thus three different measurements can be performed in one apparatus. For optimum temperature stability the apparatus is put in a vacuum jacket, which is temperature controlled by a thermostat. The pressure difference $p_C - p_D$ is measured using a differential capacitance manometer (sensitivity: 10^{-4} Pa). The pressure drops $p_A - p_C$ and $p_C - p_B$ are measured with oil manometers. The resolving power of the entire system was found to be such that at the higher pressures relative changes in the viscosity as small as 5×10^{-6} could be detected.

4. Corrections

The relations between the observed pressure differences and changes in viscosity as given in eqs. (8) through (10) are strictly valid only under ideal conditions. In the actual experimental set-up various corrections have to be taken into account. Eqs. (8) through (10) then become

$$2\frac{p_C(E)-p_D(E)}{p_A-p_B}\left\{1+\frac{1}{8}\left(\frac{p_A-p_B}{p+K_\eta}\right)^2\right\} = -\left\{(1-\epsilon_1)\frac{\Delta\eta_1^+(E)}{\eta}+\epsilon_1\frac{\Delta\eta_2^+(E)}{\eta}\right\}, \tag{11}$$

$$2\frac{p_C(B)-p_D(B)}{p_A-p_B}\left\{1+\frac{1}{8}\left(\frac{p_A-p_B}{p+K_\eta}\right)^2\right\} = -\left\{(1-\epsilon_1)\frac{\Delta\eta_1^+(B)}{\eta}+\epsilon_1\frac{\Delta\eta_2^+(B)}{\eta}-\frac{\Delta\eta_2^+(\epsilon_2 B)}{\eta}\right\}, \tag{12}$$

$$2\frac{p_D(B)-p_C(B)}{p_A-p_B}\left\{1+\frac{1}{8}\left(\frac{p_A-p_B}{p+K_\eta}\right)^2\right\} = -\left\{(1-\epsilon_1)\frac{\Delta\eta_2^+(B)}{\eta}+\epsilon_1\frac{\Delta\eta_1^+(B)}{\eta}-\frac{\Delta\eta_1^+(\epsilon_2 B)}{\eta}\right\}. \tag{13}$$

TABLE I

The Knudsen correction parameters for η, $\Delta\eta$, B/p and E/p as found in this experiment ($T = 300$ K, $t = 0.5$ mm), together with literature data on the field free viscosity. The data in parentheses are calculated according to ref. 9

Gas	K_η (Pa)	$K_{\Delta\eta(B)}$ (Pa)	$K_{\Delta\eta(E)}$ (Pa)	$K_{B/p}$ (Pa)	$K_{E/p}$ (Pa)	η (10^{-6} Pa · s)
N_2	(81)	146	—	62	—	17.8
CH_3Cl	(36)	—	64	—	12	10.7
CH_3F	(46)	20	63	19	14	11.0
CH_3F He (0.50 -0.50)	94	106	163	48	57	32.5
PF_3	(44)	66	66	31	31	16.9

The various corrections stem from

1) The expansion of the gas: The correction factor for this effect is[19])

$$\frac{1}{8}\left(\frac{p_A - p_B}{p + K_\eta}\right)^2,$$

where K_η is the Knudsen corection for the field free viscosity and p the average pressure in the bridge. The values for K_η (see table I) have been calculated[9]), except the one for CH_3F–He, which has been determined in the present experimental set-up.

2) The broadening due to the expansion of the gas: Since the viscosity is studied as a function of the field to pressure ratio, a spread in field functions will occur because of the pressure drop across the capillary. Care was taken as to regulate the flow in such a way that $\Delta p/p < 0.3$. The magnitude of this correction decreases with increasing field-to-pressure ratio and is negligible for the region of interest.

3) Pressure drops at the entrance of and inside the capillaries: A correction factor for this effect is discussed in refs. 16 and 18. For the present apparatus this correction is of the order of 10^{-3} and is therefore neglected.

4) The finite width of the capillaries: This causes a small distortion in the flow profile. The correction ϵ_1 is determined by the dimensions t and w of the capillary[18]); in our case $\epsilon_1 = 1.6 \times 10^{-2}$.

5) The viscous resistance of entrance and exit leads; and

6) the zero field unbalance of the bridge: These corrections are of the order of 10^{-3} and are neglected.

7) Magnetic stray field effects on the pair of capillaries that are not in the field centre: The fraction of the magnetic field felt at 0.62 m from the field centre is $\epsilon_2 = 7.5 \times 10^{-3}$. The magnitude of the correction for these effects depends on the B/p region studied, being 1.5×10^{-2} at most.

8) Magnetic stray field effects on the entrance and exit leads: The correction for these effects has been calculated using a simplified model for the field decay in the vertical direction[19]). The correction was found to be smaller than 10^{-3} and is therefore neglected.

9) Knudsen effects: These effects occur at low densities, when the mean free path of the molecules becomes of the same order of magnitude as the dimensions of the capillaries. Corrections must therefore be applied to the field free viscosity (see correction 1), to the magnitude $\Delta\eta/\eta$, and to the field-to-pressure ratio F/p ($F = B$ or E) of the field effects. These last two corrections are applied according to[20])

$$\frac{\Delta\eta}{\eta} = \left(\frac{\Delta\eta}{\eta}\right)_{\mathrm{m}} \left(1 + \frac{K_{\Delta\eta}}{p}\right), \tag{14}$$

$$\frac{F}{p} = \left(\frac{F}{p}\right)_{\mathrm{m}} \left(1 + \frac{K_{F/p}}{p}\right)^{-1}, \tag{15}$$

where m stands for "measured at pressure p". Values for the experimentally determined Knudsen parameters are listed in table I. The magnitudes of these corrections range from 2% to 60% for the pressures used.

5. Experimental results

Experiments were carried out at room temperature on the linear molecule N_2, the prolate molecules CH_3Cl and CH_3F, the mixture CH_3F–He and the oblate molecule PF_3. All gases were obtained commercially. The purities of the gases were all better than 99%. Some relevant properties of the various molecules are listed in table II.

TABLE II

Molecular constants (SI units): the rotational temperature $\hbar^2/2kI_\perp$, the ratio of moments of inertia $I_\parallel/I_\perp$, rotational g-factors, the electric dipole moment μ_e, the mean electric polarizability $\bar{\alpha}$ and its anisotropic part $\alpha^\parallel - \alpha^\perp$. The symbols $\parallel$ and $\perp$ refer to directions parallel and perpendicular to the molecular axis of symmetry. Most data are taken from refs. 9 and 26

Gas	$\frac{\hbar^2}{2kI_\perp}$ (K)	$I_\parallel/I_\perp$	$g_\perp$	$g_\parallel$	μ_e (10^{-30} C · m)	$\bar{\alpha}$ (10^{-40} F · m^2)	$\alpha^\parallel - \alpha^\perp$ (10^{-40} F · m^2)
N_2	2.9	0	− 0.278		0	1.97	+ 0.77
CH_3Cl	0.63	0.086	− 0.0163	+ 0.305	6.23	5.14	+ 1.8
CH_3F	1.2	0.166	− 0.062	+ 0.265	6.20	2.93	+ 0.36
PF_3	0.38	1.61	− 0.0659	− 0.081	3.44	4.59	− 0.70

The analysis of measured data begins with the correction for the expansion of the gas (correction 1). Next, Knudsen corrections are applied to the individual pressure runs, using eqs. (14) and (15). The Knudsen correction parameters are listed in table I. For CH_3F the Knudsen parameters for the electric and the magnetic field effect were found to be different. This discrepancy is probably caused by the experimental uncertainty in the determination of the saturation values of the various pressure runs for this gas. Also, contributions from rarefied gas effects[21,22]) or wall effects[23,24]) may be responsible. Since the experimental Knudsen constants listed in table I contain both the correction for real Knudsen effects and possibly also for other $1/p$-effects, they should be regarded only as a tool for obtaining the zero mean free path limit. After this extrapolation corrections 4 and 7 are applied and a check on the $\mathscr{Y}^{(2)}$-polarization is performed by plotting the ratio of $(B/p)_1$ and $(B/p)_2$ as a function of $\Delta\eta/\eta$, see e.g. fig. 4. If this ratio differs from the theoretical value 2, also another polarization is present and further investigation of the $\mathscr{Y}^{(2)}$-polarization is unreliable for our purpose.

Finally some tests on the scalar factor of the $\mathscr{Y}^{(2)}$-polarization are performed. First the individual magnetic and electric field measurements and theoretical curve-fit procedures are used to determine whether it is possible to make a choice

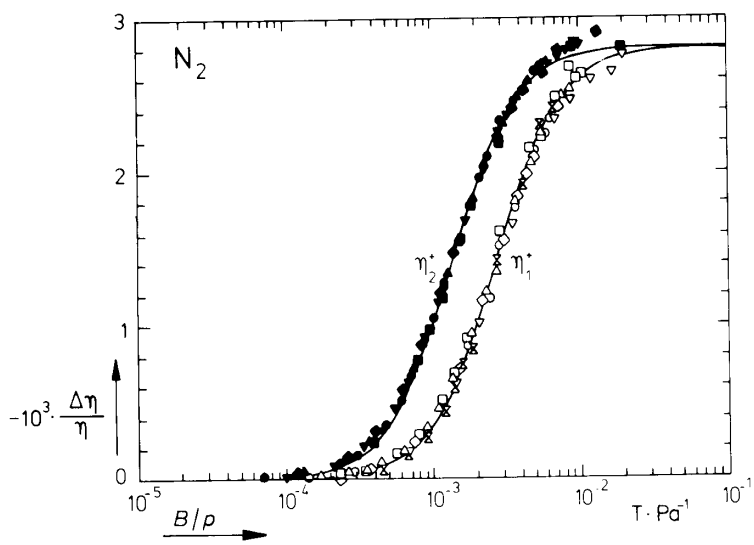

Fig. 3. $-\Delta\eta/\eta$ versus B/p for N_2. ▽ 285 Pa, □ 604 Pa, △ 780 Pa, ⧖ 785 Pa, ◇ 959 Pa, ○ 1265 Pa, ■ 340 Pa, ◆ 489 Pa, ▼ 635 Pa, ▲ 968 Pa, ● 1232 Pa. ———: theoretical curve of eq. (4) scaled to fit the experimental points. For linear molecules the precession frequency is independent of the molecular rotational state and hence the form of the scalar factor of the polarization does not play a role in the shape of the curve. The saturation value is 2.81×10^{-3} and the half field-to-pressure ratio for η_1^+ is 2.6 mT/Pa.

TABLE III

Results of the numerical analysis of data on the magnetic and electric field effects on the viscosity ($T = 300$ K). The saturation values $(\Delta\eta/\eta)_{sat}$ and the half saturation field to pressure ratios $(B/p)_{1/2}$ and $(E/p)_{1/2}$ of η_1^+ follow from a least square fit of the curves of eq. (4) to the data points. The first columns refer to $P = 1$ and the second ones to $P \sim J^2$. The indices 1 and 2 refer to η_1^+ and η_2^+, respectively

Gas	Magnetic					Electric			
	$10^3 \times \left(\frac{\Delta\eta}{\eta}\right)_{sat}$		$\left(\frac{B}{p}\right)_{1/2}$ (mT/Pa)		$\left\langle\frac{(B/p)_1}{(B/p)_2}\right\rangle$	$10^3 \times \left(\frac{\Delta\eta}{\eta}\right)_{sat}$		$\left(\frac{E}{p}\right)_{1/2}$ ($V \cdot m^{-1}$/Pa)	
N_2	− 2.8	− 2.8	2.6	2.6	2.0 ± 0.1	—	—	—	—
CH_3Cl	—	—	—	—	—	− 1.4	− 1.1	1500	1000
CH_3F	− 0.8	− 0.7	52	46	2.4 ± 0.3	− 0.8	− 0.8	690	590
CH_3F–He (0.50–0.50)	− 1.3	− 1.1	37	31	2.2 ± 0.2	− 1.1	− 1.0	300	260
PF_3	− 2.27	− 2.27	24	24	2.06 ± 0.14	− 2.28	− 2.23	190	180

of the scalar factor based on the separate curves. Then a combined fit of magnetic and electric field measurements is made (i.e., using the same parameters for both curves). As pointed out in section 2, an elegant way of comparing magnetic and electric field measurement is obtained by plotting in one single graph the ratio of B/p and E/p as a function of the degree of saturation, see e.g., fig. 17. In determining B/p for η_1^+ the values for η_2^+ were also employed by shifting them along the B/p axis by a factor 2.

Note that the saturation value for the electric field effect is generally lower than the one for the magnetic field effect, since in the electric field case the molecules for which $K = 0$ do not contribute to the effect (cf. eq. (6)).

Experimental results for the magnetic and electric field dependence of the relative change in the coefficients η_1^+ and η_2^+ are shown in figs. 3 through 17. Some experimental values are listed in table III.

6. Discussion

In this section we will discuss the results presented in the previous section.

1) N_2 (figs. 3 and 4). These measurements were carried out as a check on the apparatus. As must be expected, no electric field effect was found. The results for the magnetic field effects on η_1^+ and η_2^+ reproduce the ones obtained by Hulsman[18]). Fig. 4 shows the ratio of the field-to-pressure ratios of the two coefficients as a function of the relative change in the viscosity. This ratio should

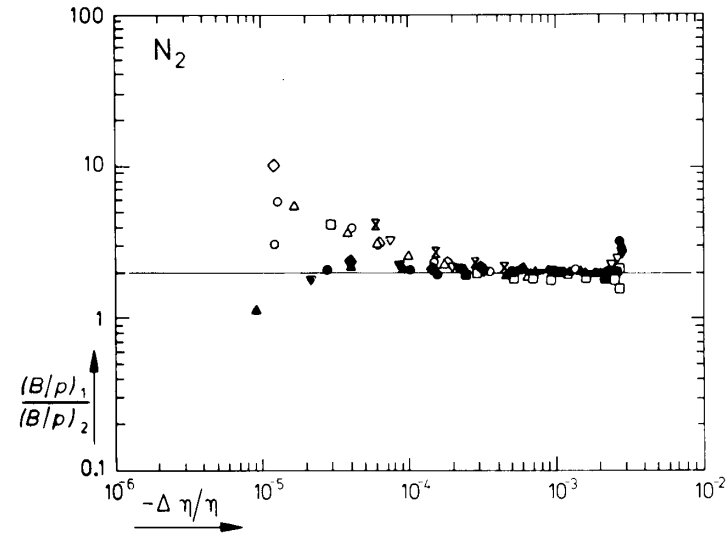

Fig. 4. $\mathscr{Y}^{(2)}$-polarization test from the magnetic field measurements for N_2. The ratio of the positions of the two sets of data points from fig. 3 are plotted as a function of the magnitude of the effect. For a $\mathscr{Y}^{(2)}$-type of polarization one expects a value 2 (see line). The symbols for the various pressure runs are the same as in fig. 3. The average of the data points is 2.0 ± 0.1.

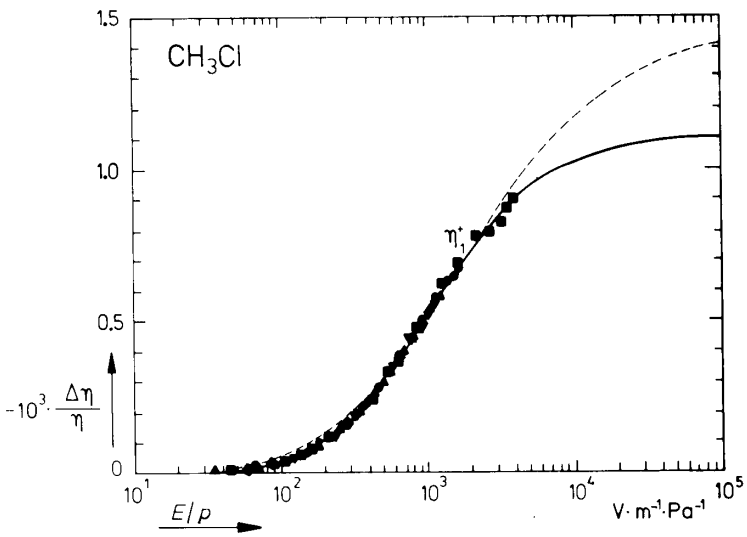

Fig. 5. $-\Delta\eta/\eta$ versus E/p for CH_3Cl. ■ 174 Pa, ● 426 Pa, ▲ 553 Pa, ▼ 628 Pa, ◆ 673 Pa, ⧗ 870 Pa. - - - -: theoretical curve of eq. (4) for $P = 1$, ———: theoretical curve of eq. (4) for $P \sim J^2$. The theoretical curves are scaled to fit the experimental points. The choices $P = 1$ and $P \sim J^2$ yield the saturation values 1.43 and 1.10, and the half saturation field-to-pressure ratios 1600 and 1000 V · m $^{-1}$/Pa, respectively.

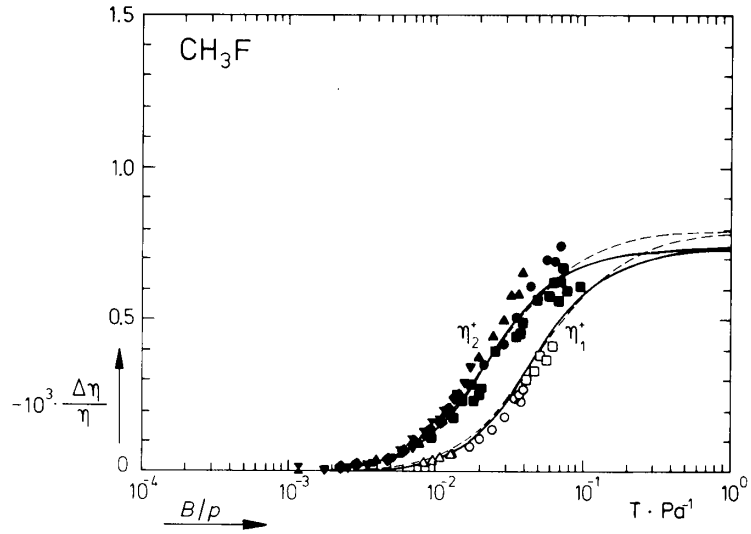

Fig. 6. $-\Delta\eta/\eta$ versus B/p for CH_3F. □ 92 Pa, ○ 173 Pa, △ 526 Pa, ■ 197 Pa, ● 273 Pa, ▲ 301 Pa, ▼ 590 Pa, ◆ 805 Pa, ⧗ 622 Pa. – – – –: theoretical curve of eq. (4) for $P = 1$, ———: theoretical curve of eq. (4) for $P \sim J^2$. The theoretical curves are scaled to fit the experimental points. The choices $P = 1$ and $P \sim J^2$ yield the saturation values 0.81 and 0.74×10^{-3}, and the half saturation field-to-pressure ratios (for η_1^+) 52 and 46 mT/Pa, respectively.

be precisely 2 if only a $\mathcal{Y}^{(2)}$-type of polarization is present. From this graph one can conclude that within the experimental error no polarization other than a $\mathcal{Y}^{(2)}$-polarization contributes to the effect for N_2.

2) CH_3Cl (fig. 5). The electric field measurements for this gas are very well described with a $\mathcal{Y}^{(2)}$ ($P \sim J^2$) polarization. As we will see below this type of agreement is not sufficient for a decisive conclusion concerning the scalar factor. No magnetic field effect could be measured due to the small g-factor and thus there is no proof that no other than a $\mathcal{Y}^{(2)}$-type of polarization is present for this gas.

3) CH_3F (figs. 6 through 9). Measurements were performed on the molecule CH_3F, because of the large difference in position of the effect between the two cases $P = 1$ and $P \sim J^2$ for this gas (see the theoretical curves in fig. 1).

Unfortunately the position of the effect proved to be such that it was not possible to measure the magnetic field effect up to high degrees of saturation. Even though the experimental uncertainty is rather large, it is clear that the distance between the two curves is systematically larger than a factor 2. This is shown in fig. 8, where this distance is plotted as a function of the magnitude of the effect. Apparently the effect cannot be described with a single $\mathcal{Y}^{(2)}$-type of polarization.

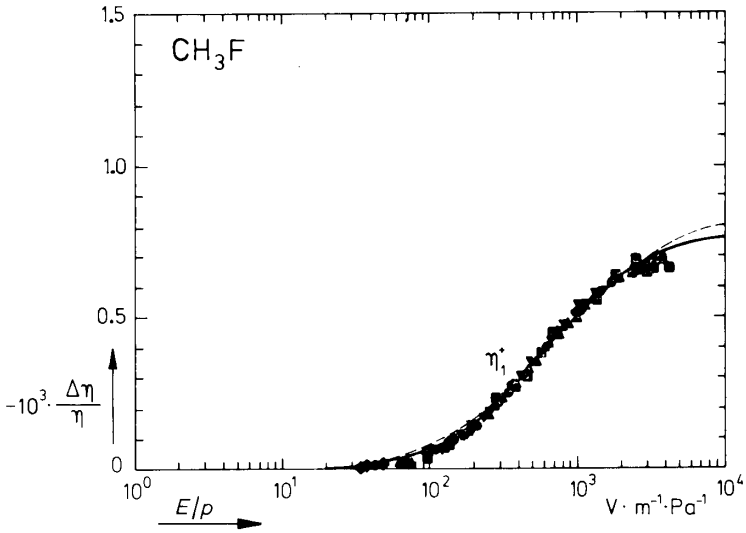

Fig. 7. $-\Delta\eta/\eta$ versus E/p for CH_3F. ■ 69 Pa, ● 88 Pa, ▲ 170 Pa, ▼ 419 Pa, ◆ 488 Pa, ⧗ 1074 Pa. – – – –: theoretical curve of eq. (4) for $P = 1$, ———: theoretical curve of eq. (4) for $P \sim J^2$. The theoretical curves are scaled to fit the experimental points. The choices $P = 1$ and $P \sim J^2$ yield the saturation values 0.83 and 0.77×10^{-3}, and the half saturation field-to-pressure ratios 690 and 590 V · m $^{-1}$/Pa, respectively.

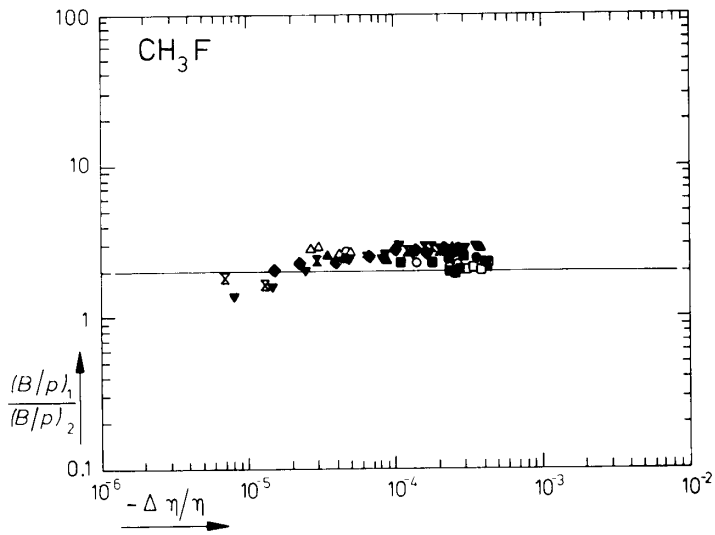

Fig. 8. $\mathcal{Y}^{(2)}$-polarization test from the magnetic field measurements for CH_3F. The ratio of the positions of the two sets of data points from fig. 6 are plotted as a function of the magnitude of the effect. For a $\mathcal{Y}^{(2)}$-type of polarization one expects a value 2 (see line). The symbols for the various pressure runs are the same as in fig. 6. The average of the data points is 2.4 ± 0.3.

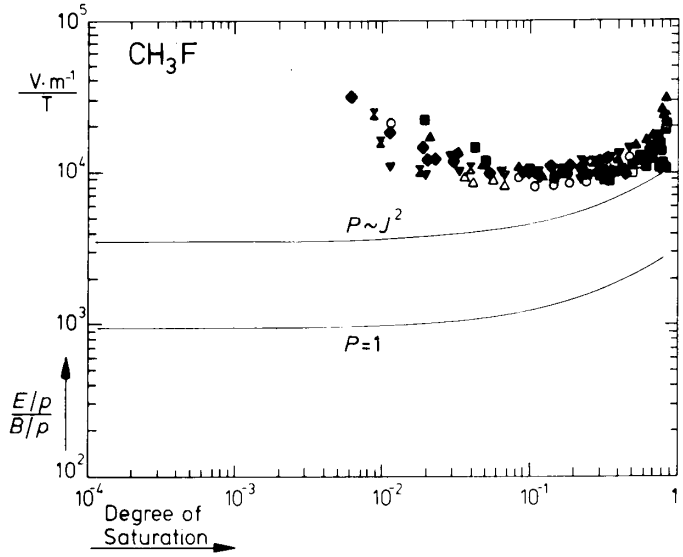

Fig. 9. Test on the scalar factor of the polarization from the magnetic and electric field measurements for CH_3F. The values of $(E/p)/(B/p)$ (from the data points for η_1^+) are plotted as a function of the degree of saturation. The symbols for the various pressure runs are the same as in figs. 6 and 7. Theoretical curves for two different choices of P for a $\mathscr{Y}^{(2)}$-polarization are shown.

Fig. 9 shows that, as expected from the presence of other polarizations, a simultaneous fit of both magnetic and electric data points fails.

According to Snider et al.[25]), in first-order distorted-wave Born approximation a dipole–dipole interaction can, for symmetric top molecules, produce a $[\boldsymbol{W}]^2\mathscr{Y}^{(1)}$-polarization, but no appreciable $\mathscr{Y}^{(2)}$-polarization, which is generally due to P_2-terms in the molecular interaction. Performing the same calculations as Snider did for NH_3 and ND_3[25]) for the production cross sections of CH_3F one indeed finds that for CH_3F not only a $\mathscr{Y}^{(2)}$-polarization but also a $[\boldsymbol{W}]^2\mathscr{Y}^{(1)}$-polarization can be expected in viscous flow.

4) CH_3F–He (0.50–0.50) (figs. 10 through 13). Measurements of an equimolar CH_3F–He mixture were performed for several reasons. In the first place dilution of CH_3F with He diminishes the dipole–dipole interaction and therefore also the contribution from the $[\boldsymbol{W}]^2\mathscr{Y}^{(1)}$-polarization. Secondly, since the sign of contributions from odd-in-$\boldsymbol{J}$ polarizations is different from the one of even-in-$\boldsymbol{J}$ polarizations, the effect is expected to increase. This would also improve the experimental accuracy. Thirdly, the position of the effect shifts towards lower B/p and E/p values, due to the fact that the decay time of the polarization, which is rather short for dipole–dipole interaction, becomes larger. This shift creates the

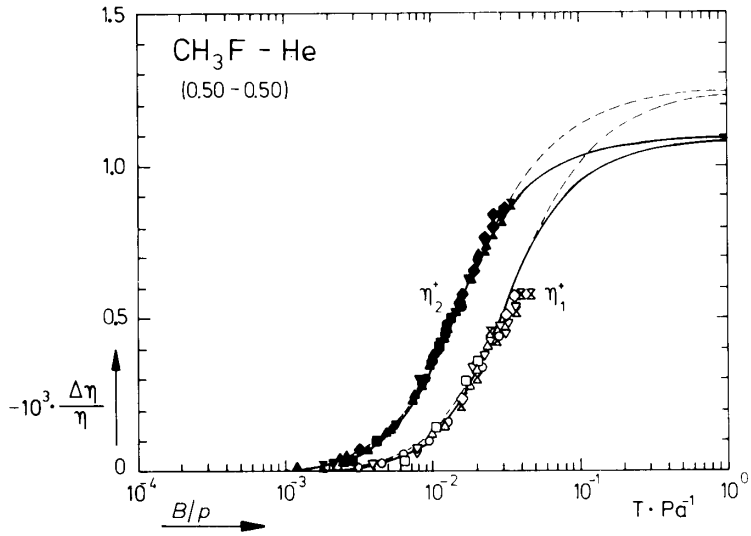

Fig. 10. $-\Delta\eta/\eta$ versus B/p for an equimolar CH_3F–He mixture. ⧖ 101 Pa, ◇ 142 Pa, ▽ 150 Pa, △ 186 Pa, ○ 196 Pa, □ 310 Pa, ⧗ 155 Pa, ◆ 187 Pa, ▼ 216 Pa, ▲ 260 Pa, ● 360 Pa, ■ 490 Pa. – – – –: theoretical curve of eq. (4) for $P = 1$, ———: theoretical curve of eq. (4) for $P \sim J^2$. The theoretical curves are scaled to fit the experimental points. The choices $P = 1$ and $P \sim J^2$ yield the saturation values 1.25 and 1.09×10^{-3}, and the half saturation field-to-pressure ratios (for η_1^+) 37 and 31 mT/Pa, respectively.

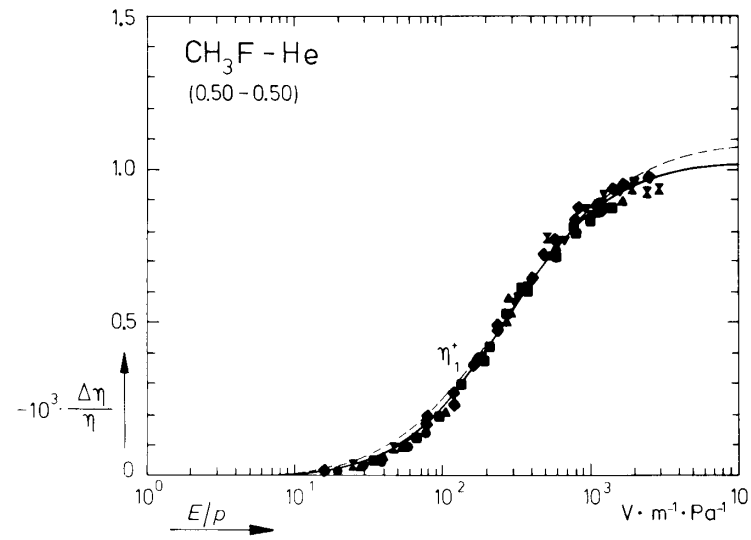

Fig. 11. $-\Delta\eta/\eta$ versus E/p for an equimolar CH_3F–He mixture. ⧗ 150 Pa, ◆ 190 Pa, ▼ 260 Pa, ▲ 310 Pa, ● 454 Pa, ■ 490 Pa. – – – –: theoretical curve of eq. (4) for $P = 1$, ———: theoretical curve of eq. (4) for $P \sim J^2$. The theoretical curves are scaled to fit the experimental points. The choices $P = 1$ and $P \sim J^2$ yield the saturation values 1.08 and 1.03×10^{-3}, and the half saturation field-to-pressure ratios 300 and 260 V · m $^{-1}$/Pa, respectively.

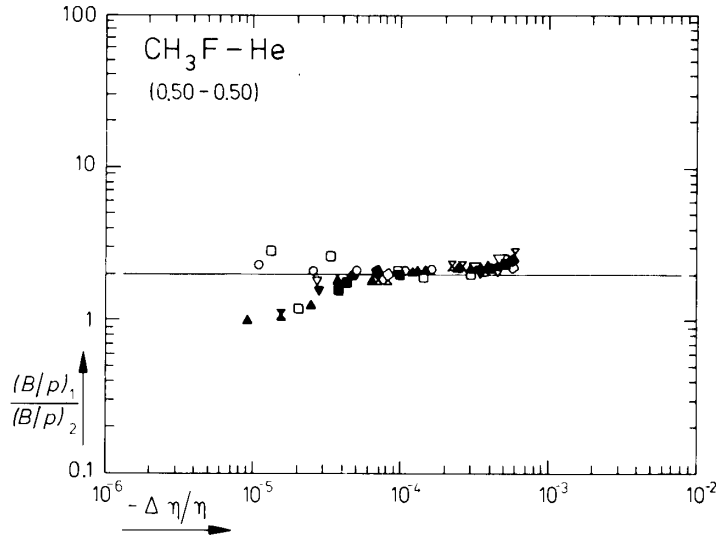

Fig. 12. $\mathscr{Y}^{(2)}$-polarization test from the magnetic field measurements for an equimolar CH_3F–He mixture. The ratio of the positions of the two sets of data points from fig. 10 is plotted as a function of the magnitude of the effect. For a $\mathscr{Y}^{(2)}$-type of polarization one expects a value 2 (see line). The symbols for the various pressure runs are the same as in fig. 10. The average of the data points is 2.2 ± 0.2.

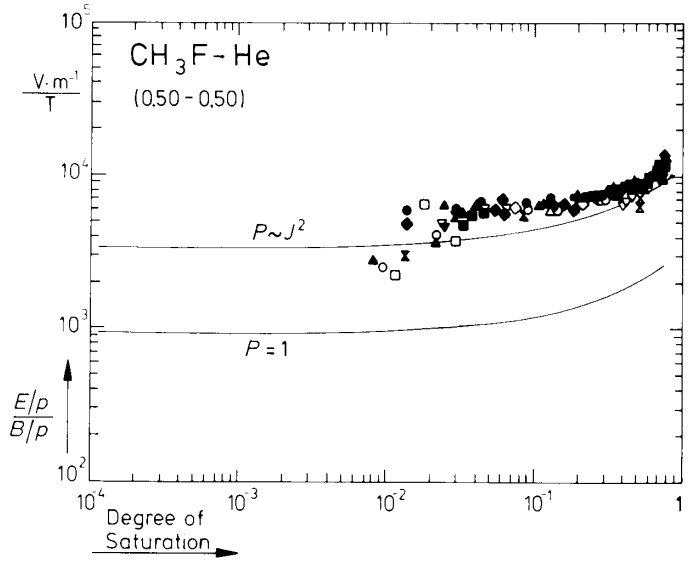

Fig. 13. Test on the scalar factor of the polarization from the magnetic and electric field measurements for an equimolar CH_3F–He mixture. The values of $(E/p)/(B/p)$ (from the data points for η_1^+) are plotted as a function of the degree of saturation. The symbols for the various pressure runs are the same as in figs. 10 and 11. Theoretical curves for two different choices of P for a $\mathscr{Y}^{(2)}$-polarization are shown.

possibility to measure up to high degrees of saturation, which results in a much higher accuracy of the analysis.

The data indeed show a higher saturation value and a lower half saturation field-to-pressure ratio and thus a higher accuracy. The ratio between the positions of the field effects for the two coefficients is now considerably closer to the value 2 (the average for the data points is 2.2 ± 0.2). Consequently, the contribution from other polarizations is clearly diminished with respect to the case of pure CH_3F (cf. figs. 8 and 12).

The magnetic field measurements are described somewhat better than for pure CH_3F by both the $P = 1$ and the $P \sim J^2$ curve (see fig. 10).

The electric measurements are described better with a $\mathscr{Y}^{(2)}$-polarization with scalar factor $P \sim J^2$ (see fig. 11). The same holds for the simultaneous fit of magnetic and electric measurements, see fig. 13. The ratio of E/p and B/p values is however systematically larger than the theoretical values for $P \sim J^2$. In view of the still detectable presence of polarizations of other tensorial type, however, no definite conclusions concerning P can be drawn.

5) PF_3 (figs. 14 through 17). Since this oblate molecule has a small dipole

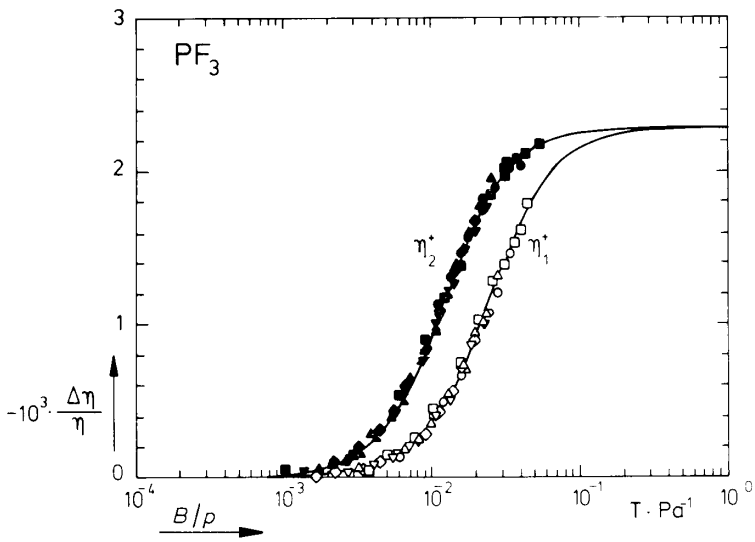

Fig. 14. $-\Delta\eta/\eta$ versus B/p for PF_3. □ 118 Pa, ○ 162 Pa, △ 203 Pa, ▽ 254 Pa, ◇ 305 Pa, ■ 93 Pa, ● 143 Pa, ▲ 182 Pa, ▼ 244 Pa, ◆ 310 Pa, ⧗ 330 Pa. The curve of eq. (4) has been scaled to fit the experimental points. For this gas the two curves corresponding to $P = 1$ and $P \sim J^2$ coincide. The saturation value is 2.27×10^{-3} and the half saturation field-to-pressure ratio for η_1^+ is 24 mT/Pa.

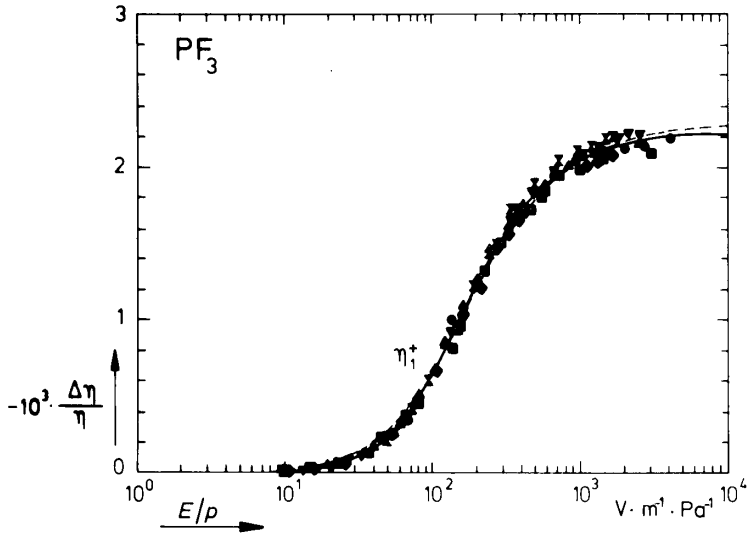

Fig. 15. $-\Delta\eta/\eta$ versus E/p for PF_3. ■ 99 Pa, ● 114 Pa, ▲ 208 Pa, ▼ 252 Pa, ◆ 333 Pa, ⧗ 376 Pa. – – – –: theoretical curve of eq. (4) for $P = 1$, ———: theoretical curve of eq. (4) for $P \sim J^2$. The theoretical curves are scaled to fit the experimental points. The choices $P = 1$ and $P \sim J^2$ yield the saturation values 2.28 and 2.23×10^{-3}, and the half saturation field-to-pressure ratios 190 and 180 $V \cdot m^{-1}/Pa$, respectively.

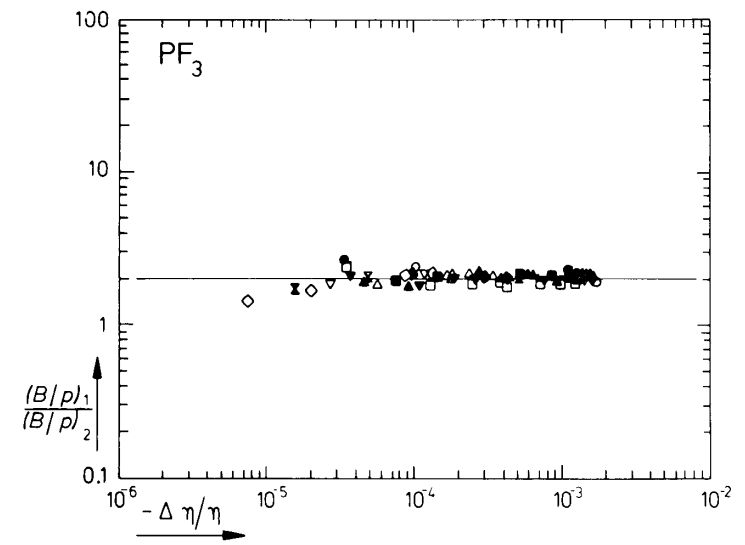

Fig. 16. $\mathscr{Y}^{(2)}$-polarization test from the magnetic field measurements for PF_3. The ratio of the positions of the two sets of data points from fig. 14 are plotted as a function of the magnitude of the effect. For a $\mathscr{Y}^{(2)}$-type of polarization one expects a value 2 (see line). The symbols for the various pressure runs are the same as in fig. 14. The average of the data points is 2.06 ± 0.14.

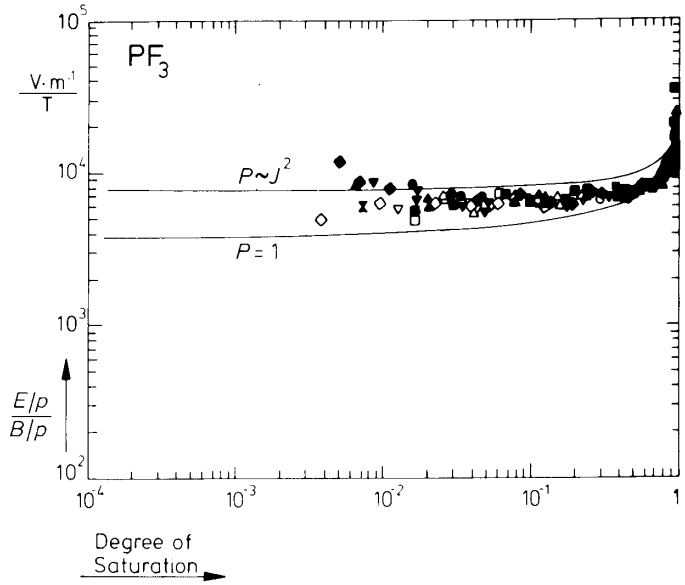

Fig. 17. Test on the scalar factor of the polarization from the magnetic and electric field measurements for PF_3. The values of $(E/p)/(B/p)$ (from the data points for η_1^+) are plotted as a function of the degree of saturation. The symbols for the various pressure runs are the same as in figs. 14 and 15. Theoretical curves for two different choices of P for a $\mathscr{Y}^{(2)}$-polarization are shown.

moment it is expected to show only the contribution from a $\mathscr{Y}^{(2)}$-type of polarization. Earlier measurements by Van Ditzhuyzen moreover showed that the viscomagnetic effect for PF_3 is very large[9]). Therefore it was decided to perform measurements on the gas PF_3, which would hopefully yield the decisive information. Indeed, the ratio between the positions of the magnetic field effects (see fig. 16) is now precisely 2. At first glance both the magnetic and the electric field measurements seem to show a perfect $\mathscr{Y}^{(2)}$ ($P \sim J^2$) behaviour (see figs. 14, 15 and 16). A simultaneous fit, however, fails again (see fig. 17): neither description satisfies the experimental points.

In conclusion we can say that neither possibility for the scalar factor of the $\mathscr{Y}^{(2)}$-polarization mentioned in section 1, namely $P = 1$ or $P \sim J^2$, describes the experimental results very well. This is especially emphasized by the measurements of PF_3, where no complications of either nature arise. These last measurements are accurate and no tensorial type other than the $\mathscr{Y}^{(2)}$-type of polarization is present. Probably one should not limit oneself to the two choices of P mentioned in section 1, but also allow a more complicated form of the scalar factor, e.g. a combination

of these two possibilities. The present experimental results, however, do not allow a more profound quantitative analysis of the scalar factor of the polarization, taking into account more than one of the possibilities studied in this paper.

Acknowledgements

The technical assistance of Mr. F.A. Robbers and Mr. P. Zwanenburg is gratefully acknowledged.

This work is part of the research program of the Stichting voor Fundamenteel Onderzoek der Materie (Foundation for Fundamental Research on Matter) and was made possible by financial support from the Nederlandse Organisatie voor Zuiver-Wetenschappelijk Onderzoek (Netherlands Organization for the Advancement of Pure Research).

References

1) J.J.M. Beenakker and F.R. McCourt, Ann. Rev. Phys. Chem. **21** (1970) 47.
2) J.J.M. Beenakker, Lecture Notes in Physics **31** (Springer, Berlin, 1974) 413.
3) H.F.P. Knaap, G.W. 't Hooft, E. Mazur and L.J.F. Hermans, Proc. 11th Symp. on Rarefied Gas Dynamics (Cannes, 1978) p. 777.
4) E. Mazur, J.J.M. Beenakker and I. Kuščer, Physica **121A** (1983) 430.
5) J.A.R. Coope, R.F. Snider and F.R. McCourt, J. Chem. Phys. **43** (1965) 2269.
6) J.A.R. Coope and R.F. Snider, J. Math. Phys. **11** (1970) 1003.
7) S. Hess and W.E. Köhler, Formeln zur Tensor-Rechnung (Palm & Enke, Erlangen, 1980) ISBN 3-7896-0046-6.
8) B.J. Thijsse, G.W. 't Hooft, H.F.P. Knaap and J.J.M. Beenakker, Physica **102A** (1980) 281.
9) P.G. van Ditzhuyzen, B.J. Thijsse, L.K. van der Meij, L.J.F. Hermans and H.F.P. Knaap, Physica **88A** (1977) 53.
10) A.C. Levi, G. Scoles and F. Tommasini, Z. Naturforsch. **25a** (1970) 1213.
11) F. Tommasini, A.C. Levi, G. Scoles, J.J. de Groot, J.W. van den Broeke, C.J.N. van der Meijdenberg and J.J.M. Beenakker, Physica **49** (1970) 299.
12) F. Tommasini, A.C. Levi and G. Scoles, Z. Naturforsch. **26a** (1971) 1098.
13) F.R. McCourt and R.F. Snider, J. Chem. Phys. **47** (1967) 4117.
14) Yu.M. Kagan and L.A. Maksimov, Sov. Phys. JETP **24** (1967) 1272.
15) H. Hulsman, E.J. van Waasdijk, A.L.J. Burgmans, H.F.P. Knaap and J.J.M. Beenakker, Physica **50** (1970) 53.
16) A.L.J. Burgmans, P.G. van Ditzhuyzen, H.F.P. Knaap and J.J.M. Beenakker, Z. Naturforsch. **28a** (1973) 835.
17) A.L.J. Burgmans, P.G. van Ditzhuyzen and H.F.P. Knaap, Z. Naturforsch. **28a** (1973) 849.
18) H. Hulsman, F.G. van Kuik, K.W. Walstra, H.F.P. Knaap and J.J.M. Beenakker, Physica **57** (1972) 501.
19) B.J. Thijsse, Thesis, University of Leiden, 1978.
20) L.J.F. Hermans, J.M. Koks, A.F. Hengeveld and H.F.P. Knaap, Physica **50** (1970) 410.
21) A.C. Levi, F.R. McCourt and J. Hajdu, Physica **42** (1969) 347.

22) A.C. Levi, F.R. McCourt and J.J.M. Beenakker, Physica **42** (1969) 363.
23) H. Hulsman, G.F. Bulsing, G.E.J. Eggermont, L.J.F. Hermans and J.J.M. Beenakker, Physica **72** (1974) 287.
24) G.E.J. Eggermont, L.J.F. Hermans, J.J.M. Beenakker and H. Vestner, Physica **91A** (1978) 365.
25) R.F. Snider, J.A.R. Coope and B.C. Sanctuary, Physica **103A** (1980) 379.
26) B.J. Thijsse, W.A.P. Denissen, L.J.F. Hermans, H.F.P. Knaap and J.J.M. Beenakker, Physica **97A** (1979) 467.